Available online at www.sciencedirect.com

ScienceDirect

Acta Materialia 61 (2013) 7534–7542

Acta MATERIALIA

www.elsevier.com/locate/actamat

Interface-directed spinodal decomposition in TiAlN/CrN multilayer hard coatings studied by atom probe tomography

Ivan Povstugar [a], Pyuck-Pa Choi [a,*], Darius Tytko [a], Jae-Pyeong Ahn [b], Dierk Raabe [a]

[a] Max-Planck-Institut für Eisenforschung, Department of Microstructure Physics and Alloy Design, Max-Planck-Str. 1, 40237 Düsseldorf, Germany
[b] Korea Institute of Science and Technology, Advanced Analysis Center, P.O. Box 131, Cheongryang, 130-650 Seoul, Republic of Korea

Received 30 January 2013; received in revised form 30 July 2013; accepted 7 August 2013
Available online 27 September 2013

Abstract

Microstructural and compositional changes in TiAlN/CrN multilayered films occurring at temperatures up to 1000 °C were studied at different length scales by a combination of atom probe tomography, transmission electron microscopy and X-ray diffraction. We observe the onset of decomposition of the multilayer structure at 700 °C via the mechanism of interface-directed spinodal decomposition of TiAlN layers, where Al atoms preferentially move toward the nearest interface and segregate there. The interface-directed mechanism later transforms into isotropic spinodal decomposition and is accompanied by intense interdiffusion between the constituting layers. Distinct compositional gradients across columnar grain boundaries (extending perpendicular to the multilayers) are detected at this stage of decomposition. Drastic differences in decomposition behavior across the film depth were observed at elevated temperatures (800–1000 °C): the layered structure completely dissolves in the near-surface part but persists in the regions distant from the surface. The influence of residual stresses caused by the sputter deposition process on the thermally induced evolution of the multilayer thin films is discussed.

Keywords: Multilayer thin films; Nitrides; Atom probe tomography (APT); Spinodal decomposition; Residual stresses

1. Introduction

Many tribological loading situations require materials with an excellent combination of mechanical contact strength and corrosion resistance that is often not attainable for conventional bulk materials. A promising approach to meet these requirements is the "bottom-up" synthesis of nanostructured materials, e.g. preparation of compositionally modulated nanoscale multilayers by physical vapor deposition (PVD) techniques [1–10]. The properties of such multilayers (both metallic and ceramic) often deviate strongly from those of the corresponding bulk materials and are essentially controlled by the high interface density. The strength and hardness of multilayer hard coatings can be substantially increased by reducing the layer thickness to the nanometer range, where in-grain deformation is size limited, and the layer interfaces act as highly effective obstacles against dislocation motion [11]. The composition, elastic constants, thicknesses of the constituent layers as well as the interfacial widths are important parameters in this context, as they determine the critical shear stress across the layer interfaces. By carefully controlling these properties, hardness values up to 5000 kg mm^{-2}, which are comparable to cubic BN and only exceeded by diamond, can be achieved in many nitride multilayer systems such as TiN/AlN [5], TiN/NbN [6] and CrN/AlN [9]. Nitride hard coatings with high Al and Cr contents also exhibit good corrosion and oxidation resistance due to the formation of a passivation layer on the surface [12–14]. Such nitride multilayers have high potential as protective coating materials of cutting tools and machine parts. However, multilayers are typically in a metastable state due to the high interface density and hence

* Corresponding author. Tel.: +49 211 6792 167; fax: +49 211 6792 333.
E-mail address: p.choi@mpie.de (P.-P. Choi).

1359-6454/$36.00
http://dx.doi.org/10.1016/j.actamat.2013.08.028

possess only limited thermal stability [15]. The operation temperatures in dry-cutting applications can reach 1000 °C [16], leading to interdiffusion and dissolution of the nanolayered structure, which usually gives rise to a substantial deterioration of the mechanical properties.

One high-performance coating systems that shows an outstanding combination of wear and oxidation resistance is multilayered TiAlN/CrN [17]. Although the microstructure and mechanical properties of TiAlN/CrN multilayers as well as their thermal evolution have been studied before [17–21], the structure–property relationships of these coatings are not well understood. First, studies of the thermal stability have been usually carried out in air, which makes it difficult to distinguish between thermal and oxidation effects. Second, almost no information is available for nitride multilayer hard coatings regarding the elemental distribution at atomic scale. However, such compositional data are necessary for understanding diffusion and decomposition phenomena occurring at elevated temperatures.

Previous studies of TiAlN/CrN coatings revealed that short-range diffusion at interfaces starts already at 500 °C, but a decrease in hardness and pronounced compositional changes begin at a temperature as high as 700 °C [17,22]. The current study is focused on the nanolayered $(Ti_{0.75}Al_{0.25})N/CrN$ hard coating synthesized by means of sputter deposition. The chosen Ti:Al ratio yields a coating with single-phase face-centered cubic (fcc) structure and superior mechanical properties [21,23]. To elucidate both structural and chemical changes in TiAlN/CrN multilayers under elevated temperatures, we employ atom probe tomography (APT) in conjunction with transmission electron microscopy (TEM) and X-ray diffraction (XRD). To reveal only thermally induced changes in multilayers and distinguish them from oxidation-related phenomena at high temperatures, multilayers were heat treated in a purified Ar atmosphere (i.e. oxidation was completely excluded). The current study focuses on temperatures up to 1000 °C, which is a typical operating range for cutting tools.

2. Experimental details

$Ti_{0.75}Al_{0.25}N/CrN$ multilayers were prepared by means of reactive DC sputter deposition on a M2 HSS (high-speed steel) substrate attached to a rotating sample holder. The substrate was polished, cleaned with acetone and ethanol, and subsequently cleaned in a deposition chamber by Ar^+ bombardment. $Ti_{0.75}Al_{0.25}$ alloy and pure Cr were used as target materials. After deposition of a Cr buffer layer on the substrate, an Ar(60 vol.%)/N_2(40 vol.%) gas mixture was supplied to the chamber for deposition of the metal nitride layers. Prior to the deposition of multilayers, a 100 nm TiAlN buffer layer was deposited, where the bias voltage and temperature of the substrate were kept at −150 V and 300 °C, respectively. Additional information about the deposition procedure can be found in Ref. [21]. The total thickness of the multilayers after deposition was about 2 μm. The Ti:Al ratio of the as-sputtered TiAlN layers determined by wavelength-dispersive electron probe microanalysis (JEOL, JXA-8500F) was found to be 2.8:1.

The substrate plate with deposited coating was cut into pieces using spark erosion to avoid undesirable heating. The cut samples were sealed into quartz ampoules with purified Ar (>99.99%) and a Ti getter and annealed at different temperatures up to 1000 °C. Further APT analyses showed no oxygen contamination of the film due to annealing. Structural characterization of the film was performed using transmission electron microscopy in scanning mode (JEOL JEM-2200FS, 200 kV) and wide-angle XRD (Co K_α radiation) operating in Bragg–Brentano geometry. APT analyses were carried out with a Cameca LEAP™ 3000X HR system, applying laser pulses of 532 nm wavelength with 250 kHz pulse frequency, ~12 ps pulse length and 0.4 nJ pulse energy. The specimen base temperature and detection rate were kept at ~60 K and 0.5%, respectively.

TEM and APT specimens were prepared using a dual-beam focused-ion beam (FIB) (FEI Helios Nanolab 600) following the lift-out procedure [24,25]. To avoid analyzing near-surface regions of the film, which might have been damaged by spark erosion, APT specimens were prepared from the region 100–300 nm below the surface unless otherwise stated. To reduce the amount of Ga implantation during FIB preparation, TEM and APT specimens were milled using 5 keV ion energy for the final preparation step. The resulting Ga contamination as analyzed by APT was <0.01 at.% for all specimens. The level of other impurities in the as-sputtered coating (predominantly oxygen stemming from the residual atmosphere inside the sputtering chamber) was directly determined from the APT mass spectra and did not exceed 0.1 at.%.

3. Results

3.1. X-ray diffraction

The as-sputtered film shows single-phase fcc (B1-type) structure according to the XRD data (Fig. 1). Only (1 1 1) and (2 2 2) Bragg peaks of the B1 structure appear in the XRD patterns. Since weak XRD peaks from the steel substrate appear as well, the pattern obviously yields structural information from the entire thickness of the film. The coating in the as-sputtered state has a fiber structure where all grains have ⟨1 1 1⟩ crystallographic orientation in the direction of film growth. The lattice parameter of the fcc phase determined from the positions of the Bragg peaks is 0.427 nm, which is slightly higher compared to bulk fcc CrN (0.414 nm) and TiN (0.424 nm) phases [26], indicating dilatation of the lattice in the growth direction. The dilatation is associated with the sputter-deposition process, which causes introduction of numerous defects due to intensive ion bombardment. As the film is attached to the substrate and is not free to expand in the in-plane direction, dilatation creates residual compressive stresses parallel to

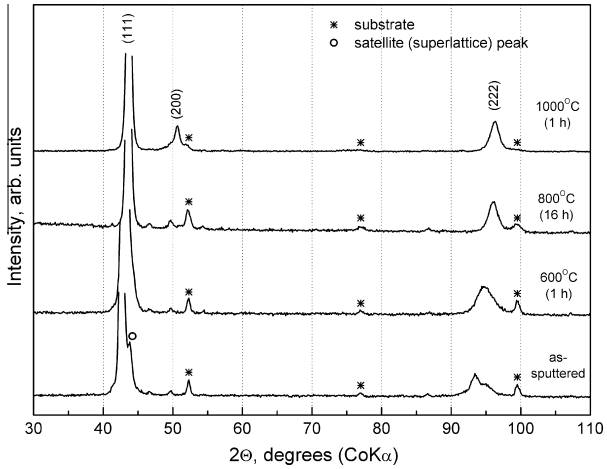

Fig. 1. X-ray diffraction patterns of the as-sputtered and annealed samples. The patterns evolve gradually with temperature and/or time in the range of 600–800 °C without any peculiarities.

the film typical for PVD coatings [27]. The bilayer period Λ of the multilayers can be estimated with the help of the superlattice (satellite) peak visible at the right-hand side of the (1 1 1) peak using the formula

$$\sin\theta_{\pm} = \sin\theta_B \pm m\lambda/2\Lambda,$$

where $2\theta_{\pm}$ and $2\theta_B$ are the positions of the satellite and Bragg peaks, respectively, m is the order of the satellite peak and λ is the X-ray wavelength [3]. The calculated Λ value is 9.2 ± 0.5 nm.

Slight changes in the XRD patterns of the film arise after annealing at 600 °C. The satellite peak disappears after 1 h annealing, indicating that the interfaces between adjacent layers become less pronounced. The fcc peaks shift toward higher angles, indicating a reduction of the lattice parameter in the growth direction due to annihilation of sputter-induced defects and, hence, release of residual stresses. The XRD patterns change gradually with the increase of annealing temperature or time. No new peaks emerge below 1000 °C, indicating high stability of the ⟨1 1 1⟩ texture and absence of recrystallization in this temperature range. The XRD pattern of the sample annealed at 1000 °C for 1 h shows an additional low-intensity peak near 51° that matches well the position of the (2 0 0) peak of the B1 structure. This may indicate the onset of recrystallization processes in the film. However, other XRD peaks characteristic for B1 structure are still absent.

3.2. Transmission electron microscopy

A TEM bright-field image of a cross-section of the as-sputtered sample, a corresponding selected-area diffraction pattern (SAED) and a high-resolution (HRTEM) image are presented in Fig. 2. Alternating TiAlN and CrN layers are clearly distinguishable due to the Z-contrast between metallic atoms. The film has a distinct columnar structure with column diameters of 20–100 nm and lengths up to several hundreds of nanometers. SAED shows all the rings characteristic of fcc structure with a random distribution of diffraction spots, pointing to random grain orientations in the direction parallel to the layers (in-plane direction). The non-uniformity of the rings emerges owing to the small aperture size used to acquire the diffraction pattern, i.e. the number of grains contributing to the SAED pattern was limited. Lattice fringes in the HRTEM image pass uninterrupted through several adjacent layers, confirming layer coherency within columnar grains. It is important to note that TEM images revealed a uniform microstructure across the entire thickness of the as-sputtered film: no difference was found between near-surface and near-substrate regions. The bilayer period determined from TEM slightly varies across the coating and is 9.0 ± 0.6 nm on average, in good agreement with the XRD data. The value obtained from TEM/XRD was used later for depth calibration of the APT reconstructions.

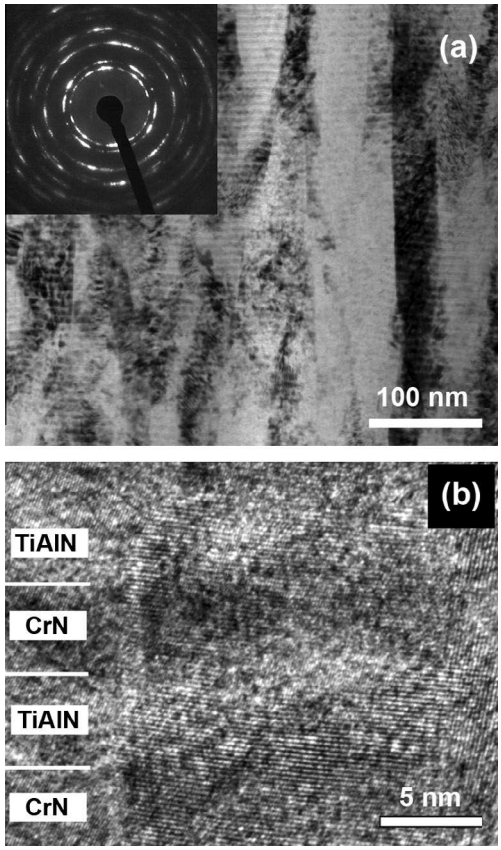

Fig. 2. (a) TEM bright-field image with corresponding electron diffraction pattern; and (b) high-resolution TEM image of the as-sputtered sample.

No notable changes in the film structure were observed by TEM at annealing temperatures below 800 °C. When this temperature is reached, the layered structure starts to dissolve gradually in the near-surface part and completely disappears after 16 h of annealing. However, the layers are still clearly visible in the region remote from the surface. The variations of the microstructure become even more pronounced after annealing at 1000 °C when the

difference in grain distribution across the film thickness becomes apparent (see Fig. 3). Numerous equiaxed grains of small size appear in the near-substrate region that may be an evidence of recrystallization processes. Such grains may contribute to the XRD (200) peak mentioned above, while their near-substrate location together with their relatively low volume fraction explains the relatively low intensity of the XRD peak.

3.3. Atom probe tomography

An APT analysis of the as-sputtered state shows alternating CrN and TiAlN layers as evidenced by the concentration profile in Fig. 4. Although TiAlN is a metastable compound across the entire compositional range [28], the TiAlN layers exhibit almost homogeneous elemental distribution. However, a careful inspection of the compositional profiles reveal that the positions of Al and Ti concentration peaks are slightly shifted with respect to each other (see Fig. 4a). Since a homogeneous Ti–Al alloy was used as a sputtering target, the shift is indicative of slight decomposition of the TiAlN layers occurring already in the PVD process. The CrN layers in the as-sputtered coating are free from Ti and Al, while TiAlN layers contain up to 3 at.% Cr. Fluctuations in nitrogen content between neighboring layers are clearly observable. While being close to the stoichiometric concentration in TiAlN layers, an obvious N deficit exists in CrN. The overall nitrogen concentration in the film is about 48 at.%, indicating the possible presence of nitrogen vacancies [29]. However, slight systematic underestimation of the N concentration (by 1–2 at.%) cannot be excluded by means of APT due to peak overlaps in the mass spectra and a high number of multiple events at the detector.

The first pronounced compositional changes are detectable by APT after annealing of the film at 700 °C for 1 h. Each of the TiAlN layers evolves into a triple-layer structure consisting of a Ti-rich layer confined by two Al-rich ones (see Figs. 4b and 5). The corresponding elemental concentration profile shows a 2-fold drop in Al concentration close to the center of the TiAlN layers compared to the as-sputtered state. Cr diffuses into TiAlN layers, resulting in an increase in Cr concentration to 8 at.%. Some diffusion of nitrogen between layers also takes place, flattening the original inhomogeneity in the N distribution. However, no in-plane concentration fluctuations within the individual layers are observed at this stage. To check the decomposition behavior in regions distant from the surface of the coating, an additional set of APT specimens was prepared from the near-substrate region (~300 nm above the buffer layer). The results of APT measurements in both regions turned out to be identical, i.e. decomposition proceeds uniformly across the entire thickness at the early stage.

An increase in annealing time or temperature causes more severe changes in the elemental distribution. Films

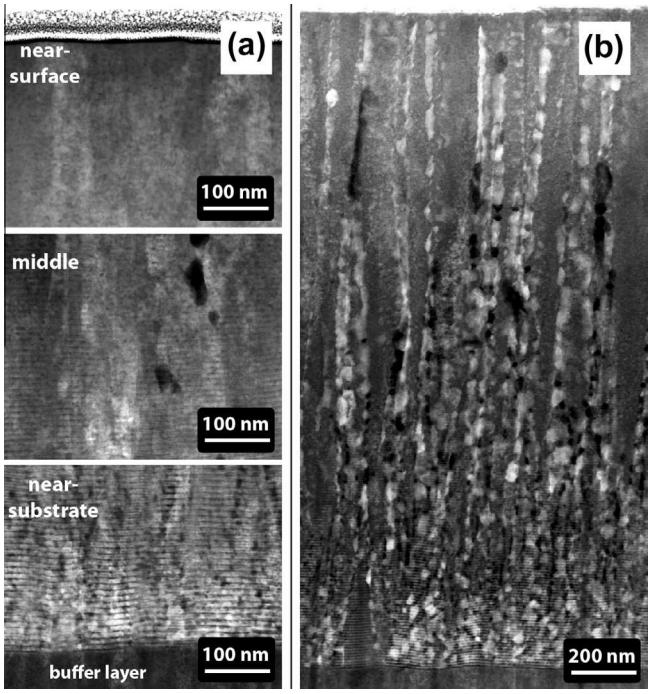

Fig. 3. Dark-field STEM images of (a) different regions of the film annealed at 800 °C for 16 h and (b) full-length cross-section of the sample annealed at 1000 °C for 1 h.

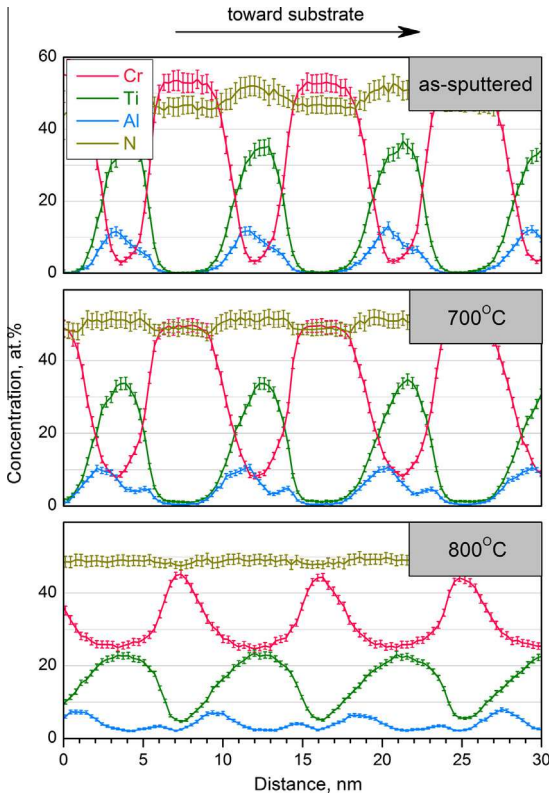

Fig. 4. Elemental concentration profiles taken across multilayers for the as-sputtered sample and samples annealed at 700 and 800 °C for 1 h. Error bars represent σ statistical error due to the limited number of atoms in a sampled volume.

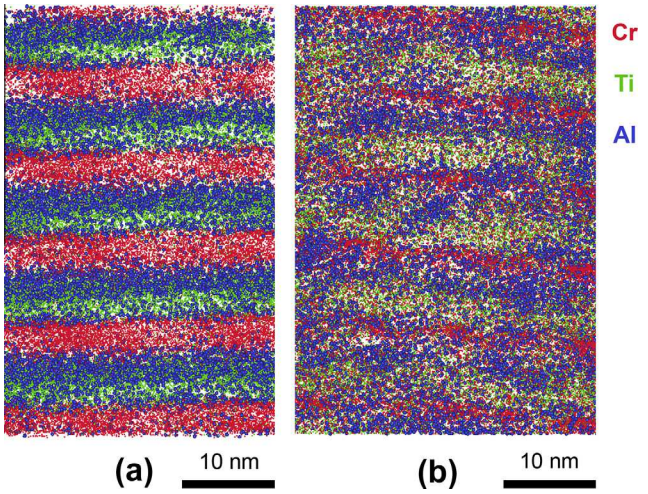

Fig. 5. APT elemental maps of the samples annealed for 1 h at (a) 700 °C and (b) 800 °C. Al atoms are shown with bigger dots to visualize decomposition patterns. N atoms are not displayed.

annealed at 800 °C for 1 h still preserve a layered structure, but numerous zones with increased Al concentration emerge inside the material (see atom map in Fig. 5b). Such an elemental distribution resembles the pattern of spinodal decomposition of thick TiAlN coatings recently studied by APT [30,31]. Additionally, planar Cr-depleted zones penetrating the entire length of the volumes analyzed by APT are visible (see Fig. 6). These zones can be identified as columnar boundaries, as their orientation and sizes of the regions between them agree well with the columnar structure observed by TEM. The chemical composition at columnar boundaries can be quantitatively characterized by in-plane concentration profiles plotted across the boundary. Fig. 6c presents a concentration profile plotted inside the CrN layers (excluding TiAlN layers from consideration) and averaged over five layers to smooth the fluctuations arising due to small sampling volumes. It is clearly seen that the CrN layers are depleted of Cr and enriched with Ti by approximately 10 at.% at the columnar boundary. Al and N concentrations do not change across the boundary. The opposite trend is observed at the edges of grains, where the Cr concentration slightly rises and the Ti concentration drops. At the same time, no compositional variations between grain boundaries and interiors were detected within adjacent TiAlN layers. This may be indicative of Ti diffusion into the CrN layers along grain boundaries and triple junctions at 800 °C, while volume diffusion remains sluggish. A similar effect in metallic multilayers, i.e. accelerated diffusion along triple lines, was recently observed by APT for the binary Fe/Cr system [32].

With increase in annealing time at 800 °C, the decomposition of the layered structure becomes increasingly pronounced, and after 4 h individual layers are barely visible. After annealing for 16 h, variations in the film structure arise even at a micrometer scale, in agreement with TEM results. The APT elemental map (Fig. 7)

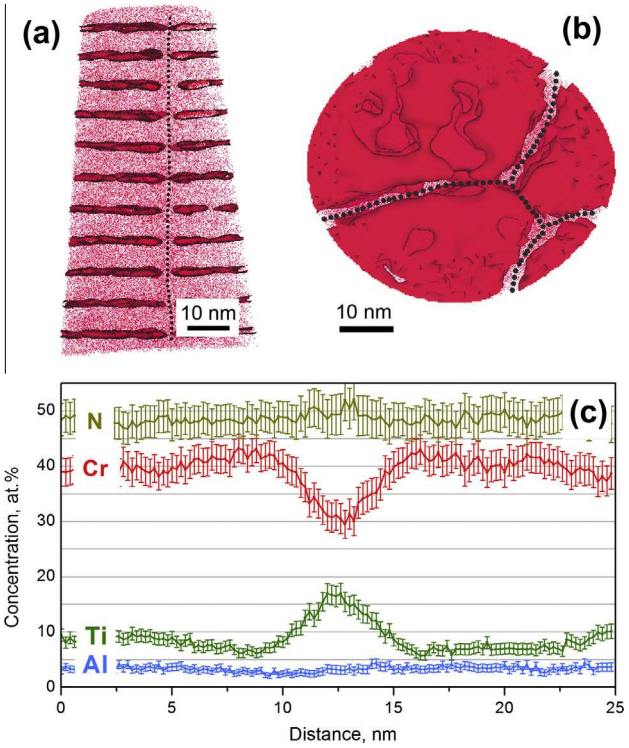

Fig. 6. (a) Side-view Cr map and 41 at.% isoconcentration surfaces of the sample annealed at 800 °C for 1 h; (b) top-view projection of the same map. Columnar boundaries are marked with dotted lines; (c) in-plane concentration profiles from interior of Cr-rich layers taken across a columnar boundary (averaged over five layers). Error bars represent σ statistical error due to limited number of atoms in a sampled volume.

evidences the absence of a layered structure in the near-surface region. Cr and Ti are fully mixed in this region of the film. A network of Al-rich zones with dimensions of about 10 nm can be clearly distinguished. At the same time, the layered structure is still resolved in the near-substrate region. Unlike earlier decomposition steps, the elemental map of the near-substrate region shows complete mixing of Cr and Ti atoms, while thin Al-rich layers with a spacing equal to the initial bilayer period (~9 nm) are distinctly visible. The concentration profile analyzed perpendicular to the layers confirms the presence of Al-rich layers. This means that the "double" Al-rich-layer structure collapses into a single layer at high temperatures within each of the original TiAlN layers. Fe and V impurities entering from the steel substrate are also observed in the near-substrate region of the film.

4. Discussion

4.1. Spinodal decomposition of TiAlN

APT results revealed that decomposition of the TiAlN/CrN multilayer structure starts from TiAlN layers, where a triple-layer structure forms with Al segregated at interfaces. This stage of decomposition proceeds continuously and uniformly across the film without any in-plane

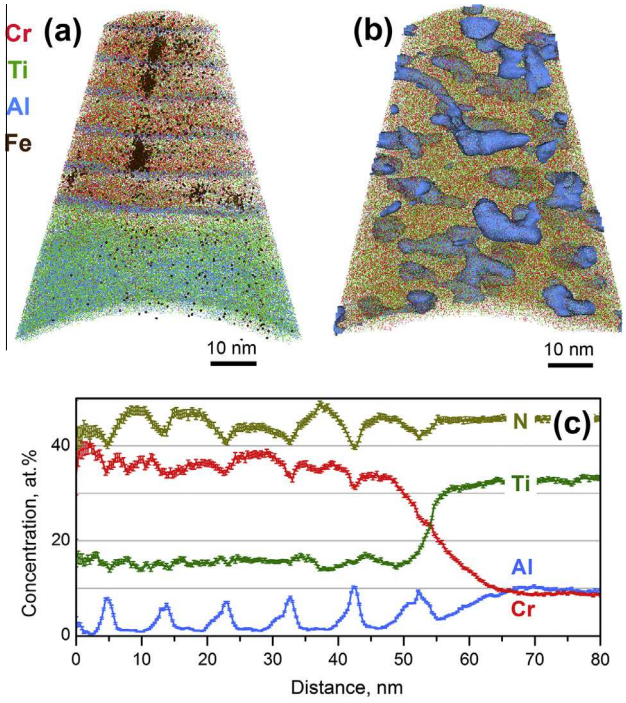

Fig. 7. APT elemental maps of the sample annealed at 800 °C for 16 h: (a) a near-surface region (Al-rich areas are decorated with 10 at.% Al isoconcentration surfaces); (b) a near-substrate region lying on the TiAlN buffer layer; (c) a concentration profile of the near-substrate region. Error bars represent σ statistical error due to the limited number of atoms in a sampled volume. Fe impurities stemming from the steel substrate are visible in the depth of the film.

fluctuation of elements. Since composition gradients are quite smooth, while XRD and TEM still show no change compared to the as-sputtered film, the decomposition does not occur via a discontinuous nucleation and growth mechanism but proceeds gradually, i.e. resembles spinodal behavior.

The thermal stability of single-phase TiAlN coatings has been extensively studied for a wide range of Ti:Al ratios both experimentally and by modeling [30,33–36]. APT investigations of relatively thick TiAlN films show elemental distribution in partially decomposed coatings, which is typical of spinodal decomposition [31]. Combined TEM and XRD studies of thermally induced structural changes in TiAlN revealed coherent regions with two slightly different lattice parameters and the presence of nanoscaled strained areas in the lattice that are also characteristic of the spinodal mechanism rather than nucleation and growth [33]. The spinodal region in TiAlN was determined by Alling et al. from first-principles calculations using two independent methods based on density functional theory [35]. The results of both methods are in a good agreement and give a spinodal concentration range extending from 20 to 99 at.% of AlN at 1000 K. Calculations performed by Mayrhofer at el. [36] give similar values for a spinodal range (27–98 at.% AlN at 900 °C). The spinodal field calculated in both works expands with decreasing temperature. It should also be noted that calculations of the spinodal range were performed in Refs. [35,36] for a fully relaxed state of the TiAlN phase and cannot be directly applied to PVD films, which are typically under high residual stresses. It was shown that the spinodal field must expand when an external pressure up to 20 GPa is applied to the TiAlN [37]. The observed small Cr impurity in TiAlN (see Section 3.3) probably does not shift the composition away from the spinodal field, as low Cr addition to TiAlN does not notably modify the calculated free energy curve of the system [38]. The non-stoichiometric nitrogen concentration due to improper deposition conditions, which have been reported to inhibit the spinodal mechanism in nitrides [10,39], is relatively small in the current study and is unlikely to have a notable influence. Based on these studies, we conclude that the $Ti_{0.75}Al_{0.25}N$ composition must stay within the spinodal field at temperatures below 800 °C, albeit being very close to its boundary. Hence, spinodal behavior should be expected for TiAlN layers in the studied coating, and the elemental distribution in the film annealed at 800 °C (see Figs. 5 and 7) gives clear support for the spinodal mechanism.

The decomposition pattern observed at earlier annealing stages, i.e. the formation of a triple-layer structure from TiAlN layers, is different from the common isotropic spinodal mechanism, as there is a clear preferential direction for uphill diffusion (perpendicular to layers). On the other hand, it resembles the so-called surface-directed spinodal decomposition discovered earlier in metallic [40], ceramic [41] and polymer [42] materials. This decomposition regime, i.e. decomposition in the presence of a free surface, has been theoretically considered and simulated by several authors, e.g. using phase-field modeling [43–45]. Anisotropic compositional modulations oriented in certain directions with respect to the surface were predicted and linked to the local bias in the free energy of the system. This bias arises due to tendency of segregation of the low-surface-energy component at the free surface, which, in turn, creates a gradient of the chemical potential perpendicular to the surface providing a preferential direction for uphill diffusion. As a result, directed (non-random) compositional waves emerge in near-surface regions, with pattern and period being dependent on the surface energy and volume mismatch between the decomposing phases. However, only a few experimental observations of surface-directed spinodal decomposition in metallic or ceramic films have been reported so far [40,41]. Since we observe this effect for interfaces in multilayers instead of a free surface in the present work, the decomposition mechanism should be rather referred to as interface-directed spinodal decomposition.

Such compositional modulations parallel to interfaces were predicted when modeling the decomposition of a $(Si,Zr)O_2$ layer on Si substrate based on the assumption that no diffusion between layers occurred [43]. The presence of modulations was explained by preferential segregation of Si at the interface, which lowers the interfacial energy, with the further mechanism being identical to

surface-directed decomposition. The same mechanism could be applicable to TiAlN/CrN multilayers, taking into account an elastic energy contribution to the free energy of the system. Since the lattice parameter for single-phase $Ti_{0.75}Al_{0.25}N$ film is bigger than for CrN under similar deposition conditions [18], the existing coherency between the adjacent layers will induce a local stress gradient at the interface. Al has the smallest atomic size in fcc nitrides compared to Cr and Ti as can be concluded from Ref. [46] where a reduction of CrAlN lattice parameter was found with an increase in Al concentration. It was also shown that decomposition of TiAlN into TiN and fcc AlN decreases the molar volume of the system [47]. As a result, Al segregation at interfaces must decrease the local lattice parameter at the interfaces, lower the elastic energy and serve as a driving force for the interface-directed mode of spinodal decomposition. However, a more consistent thermodynamic and kinetic model appears to be necessary to render the conclusions here more quantitative. A phase-field model approach similar to that applied in Refs. [43–45], where the stress term caused by difference in lattice parameters and elastic constants between TiAlN and CrN layers is introduced instead of a surface energy or surface tension terms, could be used for that purpose.

4.2. Decomposition behavior related to the distance from the surface

The gradual change in the decomposition behavior with increasing distance from the coating surface is one of the most interesting and unexpected results. The authors are unaware of any observations of such an effect in the literature.

The origin of a strong difference between close-to-surface and near-substrate regions of the TiAlN/CrN multilayer coating appears to be non-trivial. The effect cannot be ascribed to any variations in structure or primary element distribution across the depth of the coating, as they were not observed in as-sputtered multilayers or at early annealing steps. Impurities from the substrate are also ruled out as a possible reason, since Fe and V appear clustered, presumably at columnar boundaries, while the decomposition behavior is different in the entire close-to-substrate region. Loss of nitrogen at high annealing temperatures, which is typical of Cr-containing nitride phases, cannot solely explain the peculiar decomposition behavior of the studied multilayers. Nitrogen loss after annealing in the Ar-gas-filled quartz glass ampoules was indeed detected by APT. However, its level is only about 2 at.% N in the top region of the film and 4 at.% N in the depth: one could expect heavier changes in the deep region due to higher nitrogen loss, while the opposite behavior is observed (a layered structure prevails in the depth, while no layers remain in the near-surface region). A plausible explanation may come from the consideration of residual stresses in the film and their relaxation relative to the depth as shown below.

The residual stresses in PVD coatings can be generally considered as the sum of external stresses, thermal stresses due to different thermal expansion coefficients of film and substrate, and intrinsic stresses arising due to the peculiarities of PVD itself [27,48,49]. The external stresses are obviously zero in the present study, since the film is not under any external loading. The thermal stress is biaxial (parallel to the film surface), compressive for fcc TiAlN coatings deposited on high-speed steel substrates and has the value of about −1 GPa [27,48]. A close value must be valid for the studied TiAlN/CrN film, as it has a close lattice parameter and hence a similar lattice mismatch with the steel substrate. The intrinsic stresses are also compressive in the in-plane direction and may reach a few gigapascals depending on film nature and PVD conditions such as substrate bias voltage [48]. Experimental measurements of the total residual stress in TiAlN/CrN using XRD give values of −3.5 to −7 GPa, depending on deposition parameters [50].

Variations in thermal decomposition behavior across the film depth may occur due to the fact that both thermal and intrinsic stresses in as-sputtered PVD coatings typically exhibit a pronounced gradient along the growing direction, with a decrease when moving toward the surface [49,51]. Additionally, the internal stress gradient may alter during annealing due to diffusion and annihilation of defects incorporated by PVD. Such a gradient leads to a complex variation in the elastic energy through-thickness contribution to the full free energy of the system. To obtain a better insight into this issue, the internal stresses in nitride films are considered in the following.

Among the main sources of intrinsic stresses in PVD coatings are under/overstoichiometry of N, incorporation of Ar impurity in the sputtering process and substitutional defects (metal ions on N sites and vice versa) [27,48]. All these sources are influenced by short- and long-range elemental diffusion, which is activated at high temperatures and inevitably results in redistribution or annihilation of these defects, eventually releasing the residual stresses. In principle, diffusion of some defect types, such as N excess or Ar impurities can be qualitatively understood from APT data as well. APT data for both near-surface and near-substrate regions of the as-sputtered film show the same N content of 48 at.% (see Section 3.3). The sample annealed at 800 °C for 16 h shows a higher N concentration in the near-surface region of 46 at.% compared to 44 at.% in the near-substrate region. Such a decrease clearly indicates nitrogen diffusion toward the surface of the coating, which must be accompanied by formation of numerous vacancies, especially in the depth of the film. Such vacancies will cause lattice shrinkage, which is more pronounced in the near-substrate region. In other words, nitrogen diffusion indeed takes place, results in alteration of the intrinsic stress gradient and eventually in variations of local microstructure. In contrast to the N effect, the analysis of the Ar distribution reveals only subtle changes across the film depth at all annealing steps, i.e. Ar cannot be considered as the source affecting the stress gradient.

However, as mentioned before, nitrogen loss itself cannot account for the variation of decomposition behavior. The behavior can be understood when additionally considering the thermal stresses at high temperatures. While intrinsic stresses strongly decrease during annealing, the role of the thermal stress, which is minor at low temperatures, increases profoundly. At temperatures above the deposition one (300 °C) the thermal stress reverses its sign, since the substrate expands more than the nitride film. In combination with the intrinsic stress release due to nitrogen diffusion, this may even result in the reversal of the sign of the total stress in the near-substrate region, i.e. the stress becomes tensile there. This reversal could explain the decomposition pattern in the near-substrate region at temperatures $\geqslant$ 800 °C, where the direction of Al diffusion appears to reverse and forms a single Al-rich layer (see Fig. 7a) instead of a double-layered structure observed at lower temperatures (compare with Fig. 5a). To clarify this issue, a careful characterization of the residual stresses gradients has yet to be performed and coupled with an accurate analysis of elemental distribution by APT.

5. Conclusions

The $Ti_{0.75}Al_{0.25}N$/CrN multilayered film is stable up to a temperature of 600 °C, when layer interfaces start to lose chemical sharpness due to short-range diffusion. Pronounced decomposition of the film begins from diffusion of Al atoms in TiAlN layers toward the nearest interface. A triple-layer structure consisting of a Ti-rich sublayer confined by two Al-rich sublayers forms within each original TiAlN layer. This mechanism is referred to as interface-directed spinodal decomposition. The interface-directed mechanism later turns into common isotropic spinodal decomposition accompanied by intensive intermixing of Cr and Ti. A distinct compositional gradient across grain boundaries, i.e. Cr depletion in favor of Ti, emerges at this stage and is attributed to grain boundary diffusion of Ti.

Continuous annealing of the film at 800 °C or higher temperatures renders the composition non-uniform in the through-thickness direction: the layer structure completely decomposes in the near-surface region, while Al-rich layers persist close to the substrate. The effect is likely caused by a gradient in the residual stresses in PVD nitride films, which changes due to nitrogen diffusion toward the film surface as well as due to substrate expansion at high temperatures.

Acknowledgements

This work was supported by the German Research Foundation (DFG) (Contract CH 943/1-1).

References

[1] Gabe DR, Wilcox GD. Met Finish 2002;100:18.
[2] Creus J, Top EH, Savall C, Refait P, Ducros C, Sanchette F. Surf Coat Technol 2008;202:4047.
[3] Yashar PC, Sproul WD. Vacuum 1999;55:179.
[4] Ziebert C, Ulrich S. J Vac Sci Technol A 2006;24:554.
[5] Kim D-G, Seong T-Y, Baik Y-J. Surf Coat Technol 2002;153:79.
[6] Shinn M, Hultman L, Barnett SA. J Mater Res 1992;7:901.
[7] Helmersson U, Todorova S, Barnett SA, Sundgren JE, Markert LC, Greene JE. J Appl Phys 1987;62:481.
[8] Yang Q, He C, Zhao LR, Immarigeon JP. Scripta Mater 2002;46:293.
[9] Lin J, Moore JJ, Mishra B, Pinkas M, Zhang X, Sproul WD. Thin Solid Films 2009;517:5798.
[10] Veprek S, Veprek-Heijman MGJ, Karvankova P, Prochazka J. Thin Solid Films 2005;476:1.
[11] Chu X, Barnett SA. J Appl Phys 1995;77:4403.
[12] Bardi U, Chenakin SP, Ghezzi F, Giolli C, Goruppa A, Lavacchi A, et al. Appl Surf Sci 2005;252:1339.
[13] Tien S-K, Duh J-G, Lee J-W. Surf Coat Technol 2007;201:5138.
[14] Barshilia HC, Surya Prakash M, Poojari A, Rajam KS. Thin Solid Films 2004;460:133.
[15] Raveh A, Zukerman I, Shneck R, Avni R, Fried I. Surf Coat Technol 2007;201:6136.
[16] Bacci da Silva M, Wallbank J. J Mater Process Technol 1999;88:195.
[17] Wadsworth I, Smith IJ, Donohue LA, Münz WD. Surf Coat Technol 1997;94–95:315.
[18] Barshilia HC, Prakash MS, Jain A, Rajam KS. Vacuum 2005;77:169.
[19] Panjan M, Šturm S, Panjan P, Čekada M. Surf Coat Technol 2007;202:815.
[20] Luo Q, Rainforth WM, Münz WD. Scripta Mater 2001;45:399.
[21] Park J-K, Park H-J, Ahn J-H, Baik Y-J. Surf Coat Technol 2009;203:3099.
[22] Choi P-P, Povstugar I, Ahn J-P, Kostka A, Raabe D. Ultramicroscopy 2011;111:518.
[23] Kimura A, Hasegawa H, Yamada K, Suzuki T. Surf Coat Technol 1999;120–121:438.
[24] Miller MK, Russell KF, Thompson GB. Ultramicroscopy 2005;102:287.
[25] Thompson K, Lawrence D, Larson DJ, Olson JD, Kelly TF, Gorman B. Ultramicroscopy 2007;107:131.
[26] International Centre for Diffraction Data. JCPDS database, No. 11-0065 (CrN), No. 38-1420 (TiN).
[27] Oettel H, Wiedemann R, Preißler S. Surf Coat Technol 1995;74–75(Part 1):273.
[28] PalDey S, Deevi SC. Mater Sci Eng A 2003;342:58.
[29] Kelly TF. Microsc Microanal 2011;17:1.
[30] Rachbauer R, Stergar E, Massl S, Moser M, Mayrhofer PH. Scripta Mater 2009;61:725.
[31] Johnson LJS, Thuvander M, Stiller K, Odén M, Hultman L. Thin Solid Films 2012;520:4362.
[32] Stender P, Balogh Z, Schmitz G. Ultramicroscopy 2011;111:524.
[33] Mayrhofer PH, Horling A, Karlsson L, Sjolen J, Larsson T, Mitterer C, et al. Appl Phys Lett 2003;83:2049.
[34] Rachbauer R, Massl S, Stergar E, Holec D, Kiener D, Keckes J, et al. J Appl Phys 2011;110:023515.
[35] Alling B, Ruban AV, Karimi A, Peil OE, Simak SI, Hultman L, et al. Phys Rev B 2007;75:045123.
[36] Mayrhofer PH, Music D, Schneider JM. Appl Phys Lett 2007;90:029902.
[37] Alling B, Oden M, Hultman L, Abrikosov IA. Appl Phys Lett 2009;95:181906.
[38] Lind H, Forsen R, Alling B, Ghafoor N, Tasnadi F, Johansson MP, et al. Appl Phys Lett 2011;99:091903.
[39] Zhang RF, Veprek S. Mater Sci Eng A 2006;424:128.
[40] Moore KT, Johnson WC, Howe JM, Aaronson HI, Veblen DR. Acta Mater 2002;50:943.
[41] Liu J, Wu X, Lennard WN, Landheer D, Dharma-Wardana MWC. J Appl Phys 2010;107:123510.
[42] Bruder F, Brenn R. Phys Rev Lett 1992;69:624.
[43] Kim H, McIntyre PC. J Appl Phys 2002;92:5094.
[44] Das SK, Puri S, Horbach J, Binder K. Phys Rev E 2005;72:061603.
[45] Wise SM, Kim JS, Johnson WC. Thin Solid Films 2005;473:151.

[46] Kimura A, Kawate M, Hasegawa H, Suzuki T. Surf Coat Technol 2003;169–170:367.
[47] Rogström L, Ullbrand J, Almer J, Hultman L, Jansson B, Odén M. Thin Solid Films 2012;520:5542.
[48] Kamminga JD, de Keijser TH, Delhez R, Mittemeijer EJ. J Appl Phys 2000;88:6332.
[49] Daniel R, Martinschitz KJ, Keckes J, Mitterer C. Acta Mater 2010;58:2621.
[50] Lewis DB, Wadsworth I, Münz WD, Kuzel Jr R, Valvoda V. Surf Coat Technol 1999;116–119:284.
[51] Machunze R, Janssen GCAM. Surf Coat Technol 2008;203:550.